Impact of nuclear effects on weak pion production at energies below 1 GeV

Jan T. Sobczyk
Fermi National Accelerator Laboratory, Batavia, Illinois 60510, USA and
Institute of Theoretical Physics, Wrocław University, pl. M. Borna 9, 50-204 Wrocław, Poland

Jakub Żmuda*
Institute of Theoretical Physics, Wrocław University, pl. M. Borna 9, 50-204 Wrocław, Poland
(Received 5 November 2012; revised manuscript received 18 April 2013; published 26 June 2013)

Charged-current single-pion production in scattering off ^{12}C is investigated for neutrino energies up to 1 GeV. A model of Nieves *et al.* [Phys. Rev. C **83**, 045501 (2011)] is further developed by performing exact integration and avoiding several approximations. The effect of exact integration is investigated both for double-differential and total neutrino-nucleus cross sections. The impact of nuclear effects with in-medium modifications of the $\Delta(1232)$ resonance properties as well as an effective field theory nonresonant background contribution are discussed. The dependence of the fraction of $\Delta(1232)$ decays into n-particle–n-hole states on incident neutrino energy is estimated. The impact of various ingredients of the model on the ratio of muon to electron neutrino cross sections is investigated in detail.

DOI: 10.1103/PhysRevC.87.065503 PACS number(s): 13.15.+g, 25.30.Pt, 24.10.Cn

I. INTRODUCTION

There has been a lot of effort to understand better single-pion-production (SPP) reactions in neutrino-nucleon and neutrino-nucleus scattering. Motivations for these studies come from the neutrino oscillation experiments and their demand to reduce systematic errors. In the few-GeV energy region characteristic of experiments such as T2K, MINOS, NOvA, MiniBooNE, and MicroBooNE the SPP channels account for a large fraction of the cross section (e.g., at 1 GeV on an isoscalar target about 1/3 of the cross section).

In a typical neutrino oscillation experiment one aims at the reconstruction of the interacting neutrino energy spectrum. In the case of charged-current (CC) interactions often one has access only to the information about the outgoing lepton kinematics. The neutrino energy is then evaluated by assuming that charged-current quasielastic (CCQE) scattering took place on a single nucleon at rest. If interactions were CCQE, this method produces a distribution narrowly peaked near the true neutrino energy with a smearing caused by Fermi motion and a possible small shift due to binding energy. For other types of interactions this method introduces a strong bias. Thus it is important to estimate the size of non-CCQE background events which may mimic the true CCQE ones.

For the neutrino energies under consideration the background is believed to be formed mainly from the SPP events with pions absorbed in nuclei and from the two-body current mechanism (two-particle–two-hole excitations, 2p2h), in which a neutrino interacts with two nucleons. The latter is often generalized to n-nucleon excitations through n-body currents ($np n$h). The impact of $np n$h effects on neutrino oscillation analysis has been evaluated by several groups in a series of papers [1]. Pion final-state interactions (FSI) were discussed in this context in Ref. [2]. Since one can effectively model nucleon-nucleon interactions by a virtual meson exchange, there exists a close relation between theoretical models for SPP and $np n$h dynamics. One of the instances of such a correlation is the possibility of in-medium decay of the $\Delta(1232)$ resonance, mediating a major part of SPP for $E_\nu < 1$ GeV. In nuclear matter this resonance may be absorbed by a pair or triplet of nucleons, leading to multinucleon excitations. This phenomenon is sometimes called the pionless Delta decay (PDD). In some of the widely used neutrino Monte Carlo (MC) generators (e.g., NEUT and NUANCE) PDD has been implemented as a constant fraction of about 20% of the total Δ production.

Another well-known instance of the relevance of pion production channels in neutrino oscillation analysis is the neutral-current π^0 production. The neutral pions give rise to events which can mimic the $\nu_\mu \to \nu_e$ signal. This occurs if one of the two photons from the π^0 decay remains undetected and the second one is misidentified as coming from an electron.

In this paper we focus on neutrino energies below 1 GeV, where SPP is dominated by the intermediate Δ resonance excitation. There are several challenges in the theoretical description of SPP reactions. The first one comes from uncertainties in the $N\Delta$ transition matrix element. The vector part is well established thanks to photo- and electroproduction experiments, but precise information on its axial counterpart is still missing. In order to describe all SPP channels simultaneously one needs to add nonresonant background amplitudes. Several models of the background in electro- and neutrinoproduction exist (e.g., [3–7]). The first two references [3,4] contain somewhat *ad hoc* sets of Born SPP terms; the latter are based on more consistent field-theoretical approaches. Special attention will be given to the chiral model of [5]. Another problem is that the way of describing the Δ resonance propagator and decay vertex differs from model to model. The extracted Δ production form factors also differ with respect to how one defines "Delta" and "background" contributions.

In SPP on atomic nuclei several many-body effects become relevant. The most important nuclear effects going beyond

*jazmuda@ift.uni.wroc.pl

Fermi motion and Pauli blocking are related to Δ in-medium self-energy. Its real part shifts the Δ pole, whereas its imaginary part corresponds to the medium-modified SPP and PDD processes. The problem of CC SPP on nuclei has been addressed in Refs. [8–10] by assuming a Δ dominance model with many-body effects taken from Ref. [11]. The computations have shown a significant reduction of the pion production cross section. The above-mentioned calculations did not include a nonresonant background. They lead to the conclusion that a fraction of Δ pionless decays has a rather mild dependence on the incident neutrino energy.

Experimental research of the weak SPP processes is also a remarkable challenge. The models of Δ excitation matrix elements and nonresonant background are still validated mainly on old low-statistics bubble chamber experiments performed at Argonne National Laboratory (ANL, [12,13]) and Brookhaven National Laboratory (BNL, [14]). The nonresonant background is more important in both neutrino–neutron SPP channels where the cross sections are smaller than for neutrino-proton SPP reaction and the statistical uncertainties are larger. Recent experimental results on the charged-current SPP reactions on atomic nuclei come mainly from the K2K [15,16] and MiniBooNE experiments [17,18]. Unfortunately, the analysis of the underlying fundamental physical processes of pion production on nucleons is obscured by nuclear effects. There is an important impact of the nuclear medium on the primary interaction as well as on a redistribution of exclusive channels by FSI. The latter effect is usually divided into pion rescattering, absorption, charge exchange, and production of additional pions (for sufficiently high energies). These nuclear physics uncertainties are so large that the MiniBooNE Collaboration did not attempt to measure the characteristics of neutrino-*nucleon* SPP process and published the cross sections results with all the nuclear effects included (for which the signal events are those with a single pion leaving a nucleus).

Our main goal is to discuss thoroughly theoretical models of pion productions used in the current attempts to understand available experimental data. As said before, they should also be used in the estimation of non-CCQE contamination in CCQE-like samples of events, allowing for better insight into the neutrino oscillation phenomenon. For this purpose the impact of various ingredients of the model on the final results is discussed in detail. We will discuss the role of the nonresonant background contribution and recalculate the $np\pi h$ contribution coming from the pionless Δ decays as well as the simplest nuclear effects: Fermi motion and Pauli blocking. Special attention is given to the ν_μ/ν_e and $\overline{\nu}_\mu/\overline{\nu}_e$ cross-section ratios, which can be very important for $\nu_\mu \to \nu_e$ oscillation signal analysis. Our results are presented in the form of tables of total cross sections for both muon and electron (anti)neutrinos on a carbon target and neutrino energies up to 1 GeV. We calculate these cross sections separately with different approximations of nuclear effects and for separate pion charge channels. This format allows for a use in the evaluation of the systematic errors by experimental groups.

In this paper the model of weak SPP on nucleons based on Ref. [5] is used for the neutrino-nucleus scattering following the approach of Ref. [19]. The model contains a nonresonant background based on a consistent effective field theory and thus it seems to be more reliable than the models presented in [4] or [3]. Our most important contribution is a prescription of how to perform many integrals in an exact way. Thanks to that we avoid approximations that are not easy to control.

The Δ excitation vector form factors are taken from Ref. [20]. We use the dipole approximation for the axial form factor C_5^A and Adler's relation to determine C_4^A. In most of the cases we use a standard Rarita-Schwinger spin-3/2 propagator and decay width calculated from the relativistic $\pi N \Delta$ Lagrangian. The nonperturbative medium modifications are applied only to SPP diagrams containing the Δ resonance with in-medium self-energy following the parametrization of Ref. [11]. Nonperturbative medium effects (spectral functions) are not included in the nonresonant background terms (which comprise 28 independent amplitudes) due to theoretical and numerical difficulties.

We compare the predictions of our model with the recent MiniBooNE SPP data [17,18]. Our calculations are not yet a part of any MC generator and we used a simplified FSI model with constant absorption and charge exchange reaction probabilities. Under these simplified conditions we find that the model seems to have problems similar to those of other approaches in explaining the size of neutral pion production.

Our main discoveries are as follows. It turns out that the numerical approximations used in Ref. [19] do not work well in the case of double-differential cross sections, while the total cross sections produce results close to the exact ones. The ratio of muon to electron (anti)neutrino total cross section does not depend on the medium modifications of the $\Delta(1232)$ resonance. We have found out that the assumption of a constant fraction of pionless Δ decay cannot be applied for experiments with large flux contribution from $E_\nu < 1$ GeV.

The paper is organized as follows: in Sec. II we discuss the general formalism of SPP on atomic nuclei. The dynamical model of SPP is reviewed in Sec. II A and nuclear medium effects are discussed in Sec. II A1. In Sec. III we briefly introduce the numerical procedures and in Sec. IV we present our main results. Finally, Sec. V contains the conclusions.

II. THEORETICAL DESCRIPTION OF PION NEUTRINO PRODUCTION ON ATOMIC NUCLEI

The theoretical approach presented in this paper is based on the general scheme described in Ref. [19]. The basic cross-section formula for the electromagnetic or weak charged-current lepton-inclusive differential cross section with respect to the final lepton energy E' and solid angle Ω' is

$$\begin{aligned} \frac{d^3\sigma}{d\Omega' dE'} &= F_l(Q^2)\frac{|\mathbf{l}'|}{|\mathbf{l}|}\int d^3r L_{\mu\nu}W^{\mu\nu}(\rho(\mathbf{r})), \\ F_l(Q^2) &= \begin{cases} \frac{2\alpha^2}{Q^4}, & \text{electrons}, \\ \frac{G_F^2\cos^2\theta_C}{4\pi^2}, & \text{neutrinos}, \end{cases} \\ L_{\mu\nu} &= \begin{cases} l_\mu l'_\nu + l'_\mu l_\nu - g_{\mu\nu} ll', & \text{electrons}, \\ l_\mu l'_\nu + l'_\mu l_\nu - g_{\mu\nu} ll' \pm i\epsilon_{\mu\nu\alpha\beta} l'^\alpha l^\beta, & \text{neutrinos}. \end{cases} \end{aligned} \tag{1}$$

In the leptonic tensor $L_{\mu\nu}$ the $+$ sign is used for neutrinos and the $-$ sign for antineutrinos. For the weak interactions the Fermi constant is $G_F = 1.1664 \times 10^{-11}/\mathrm{MeV}^2$ and the cosine of the Cabbibo angle is $\cos(\Theta_C) = 0.974$. Furthermore, l^μ and l'^μ denote initial and final lepton four-momenta, and $q^2 = -Q^2 = (l - l')^2$ is the squared four-momentum transfer. In the laboratory frame we assume the momentum transfer to be directed along the Z axis and the scattering to take place in the X-Z plane. The local density approximation (LDA) is adopted with $\rho(\mathbf{r})$ being the nuclear matter density at the point $\mathbf{r}$. The parametrization we use in the numerical computations and several other technical details are given in Appendix B.

The cross section can be reexpressed in terms of the gauge boson self-energy in the nuclear medium, as is readily done by the substitution

$$L_{\mu\nu} W^{\mu\nu}(\rho(\mathbf{r})) = -\frac{1}{\pi} \Im[L_{\mu\nu} \Pi^{\mu\nu}(q, \mathbf{r})]. \tag{2}$$

The polarization tensor $\Pi^{\mu\nu}$ has the dimensions of (energy).[3] After multiplying it by appropriate external couplings and performing the spatial d^3r integration one gets a representation of the gauge boson self-energy. It can be evaluated by adding the contributions from Feynman diagrams representing various processes, with nucleon loops having momentum cutoffs given by the local Fermi momentum.

A dominant SPP part is in the many-body language denoted as 1p1h1π (i.e., contributions from 2p2h1π and more complicated final states are assumed to be small): there is one pion and one nucleon-hole pair (1p1h) in the final state. The corresponding contribution to the polarization tensor describing production of a pion with four-momentum k on a nucleon with four-momentum p can be represented as

$$\begin{aligned} -i\,\Pi^{\mu\nu}_{\mathrm{1p1h1}\pi}(q, \mathbf{r}) = \sum_{\text{isospin}} \int \frac{d^4p}{(2\pi)^4} \int \frac{d^4k}{(2\pi)^4} i D_\pi(k) \\ \times i G_N(p, \mathbf{r}) i G_{N'}(p + q - k, \mathbf{r}) \\ \times \mathrm{Tr}\big[A^{\mu\nu}_{\mathrm{1p1h1}\pi}(p, q, k)\big]. \end{aligned} \tag{3}$$

The hadronic tensor $A^{\mu\nu}_{\mathrm{1p1h1}\pi}$ is defined as

$$\begin{aligned} A^{\mu\nu}_{\mathrm{1p1h1}\pi} = \sum_{s,s'} \big\langle N'(p', s')\pi(k) \big| j^\mu_{cc} \big| N(p, s) \big\rangle^* \\ \times \big\langle N'(p', s')\pi(k) \big| j^\nu_{cc} \big| N(p, s) \big\rangle. \end{aligned} \tag{4}$$

In (3) G_N denotes the nucleon propagator:

$$\begin{aligned} G_N(p, \mathbf{r}) = \frac{1}{p^0 + E(p) + i\epsilon} \left(\frac{n_N(\mathbf{p}, \mathbf{r})}{p^0 - E(p) - i\epsilon} \right. \\ \left. + \frac{1 - n_N(\mathbf{p}, \mathbf{r})}{p^0 - E(p) + i\epsilon} \right), \end{aligned} \tag{5}$$

with $n_N(\mathbf{p}, \mathbf{r})$ being the occupation numbers for nucleon of isospin N. In the local Fermi gas (LFG) model $n_N(\mathbf{p}, \mathbf{r})$ is a Heaviside step function $\Theta(|\mathbf{p}| - k_F^N(\mathbf{r}))$. We are working always within the local LFG framework and from now on we will remove the $\mathbf{r}$ index from notation in order to make the equations more compact. For the same reason we will not write down explicit sums over isospins. The pion propagator is defined as

$$D_\pi(k) = \frac{1}{k^2 - m_\pi^2 + i\epsilon}. \tag{6}$$

The $\langle N'(p', s')\pi(k)| j^\mu_{cc} |N(p, s)\rangle$ are transition amplitudes between the initial nucleon state with spin s and four-momentum p and the final state containing a pion with four-momentum k and a nucleon with four-momentum $p = p + q - k$ and spin s'. After inserting the nucleon propagators into the polarization tensor we obtain the following expression:

$$\begin{aligned} -\frac{1}{\pi} \Im\big(\Pi^{\mu\nu}_{\mathrm{1p1h1}\pi} L_{\mu\nu}\big) \\ = \int \frac{d^3p}{(2\pi)^3} \int \frac{d^3k}{(2\pi)^3} \frac{1}{8 E_\pi(k) E(p) E(p')} \\ \times L_{\mu\nu} \mathrm{Tr}\big[A^{\mu\nu}_{\mathrm{1p1h1}\pi}(p, q, k)\big] \\ \times \{n_N(p)[1 - n_{N'}(p')] + n_{N'}(p')[1 - n_N(p)]\} \\ \times \delta(E(p') - q^0 + E_\pi(k) - E(p)) \end{aligned} \tag{7}$$

with the nucleon energy $E(p) = \sqrt{\mathbf{p}^2 + M^2}$ and the final pion energy $E_\pi(k) = \sqrt{\mathbf{k}^2 + m_\pi^2}$. Taking into account that the pion may carry a charge and that the nucleus atomic number can be changed, one can establish the threshold-corrected energy transfer (as for the quasielastic peak):

$$\tilde{q}^0 = q^0 - Q_{\mathrm{corr}} + \Delta_{E_F}, \quad \Delta_{E_F} \equiv E_F^N - E_F^{N'}. \tag{8}$$

In this way one accounts for the difference of rest masses of isobars by subtracting the rest mass difference Q_{corr} and for the different Fermi levels of protons and neutrons by including the difference between initial E_F^N and final Fermi energies $E_F^{N'}$. We substitute $q^0 \to \tilde{q}^0$ everywhere in the hadronic part of the polarization tensor. An alternative approach for the nuclear binding energy is used in [19] and shortly explained in Appendix B. In isospin-symmetric nuclei such as ^{12}C the exchange part of the cross section given by the terms with $n_{N'}(p')[1 - n_N(p)]$ is negligibly small and we neglect it.

A. Dynamics of single-pion production

The dynamics is defined by a set of Feynman diagrams (Fig. 1) with vertices determined by effective chiral field theory [5]. The same set of diagrams describes also pion electroproduction, with the exception of the pion pole (PP) diagram, which is purely axial [Fig. 1(g)].

After performing the summations over nucleon spins we can rewrite the hadronic tensor (4) as

$$A^{\mu\nu} = \mathrm{Tr}[(\not{p} + M)\gamma^0 s^{\mu\dagger} \gamma^0 (\not{p}' + M) s^\nu]. \tag{9}$$

The reduced-current matrix elements s^μ correspond to weak transition amplitudes:

$$\big\langle N'(p', s')\pi(k) \big| j^\mu_{cc} \big| N(p, s) \big\rangle = \bar{u}_{s'}(\boldsymbol{p}') s^\mu u_s(\boldsymbol{p}). \tag{10}$$

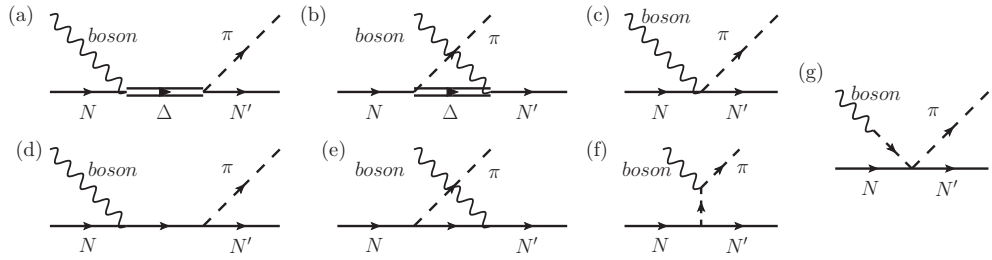

FIG. 1. Basic pion production diagrams from [5]: (a) Delta pole (ΔP), (b) crossed Delta pole (CΔP), (c) contact term (CT), (d) nucleon pole (NP), (e) crossed nucleon pole (CNP), (f) pion-in-flight (PIF), and (g) pion pole.

They are calculated to be (see [5])

$$s^{\mu}_{\Delta P} = iC_{\Delta P}\frac{f^*}{m_\pi}\cos\Theta_C k^\alpha G_{\alpha\beta}(p+q)\Gamma^{\beta\mu}(p,q), \quad (11)$$

$$s^{\mu}_{C\Delta P} = iC_{C\Delta P}\frac{f^*}{m_\pi}\cos\Theta_C \gamma^0[\Gamma^{\alpha\mu}(p-k,-q)]^\dagger\gamma^0 \times G_{\alpha\beta}(p-k)k^\beta, \quad (12)$$

$$s^{\mu}_{NP} = -iC_{NP}\frac{g_A}{\sqrt{2}f_\pi}\cos\Theta_C \not{k}\gamma^5 \times \frac{(\not{p}+\not{q}+M)}{(p+q)^2-M^2+i\epsilon} j^{\mu}_{CCN}(q)F_\pi(k-q), \quad (13)$$

$$s^{\mu}_{CNP} = -iC_{CNP}\frac{g_A}{\sqrt{2}f_\pi}\cos\Theta_C j^{\mu}_{CCN}(q) \times \frac{(\not{p}-\not{k}+M)}{(p-k)^2-M^2+i\epsilon}\not{k}\gamma^5 F_\pi(k-q), \quad (14)$$

$$s^{\mu}_{CT} = -iC_{CT}\frac{1}{\sqrt{2}f_\pi}\cos\Theta_C\gamma^\mu F_\pi(k-q) \times \left[g_A F^V_{CT}(q^2)\gamma^5 - F_\rho((q-k)^2)\right], \quad (15)$$

$$s^{\mu}_{PIF} = -iC_{PIF}\frac{g_A}{\sqrt{2}f_\pi}\cos\Theta_C F^V_{PIF}(q^2) \times \frac{(2k^\mu - q)}{(k-q)^2-m_\pi^2}2M\gamma^5 F_\pi(k-q), \quad (16)$$

$$s^{\mu}_{PP} = -iC_{PP}\frac{1}{\sqrt{2}f_\pi}\cos\Theta_C F_\rho(k-q)\frac{q^\mu \not{q}}{q^2-m_\pi^2}. \quad (17)$$

In our notation $f^* = 2.16$ is the $\pi N\Delta$ coupling constant. This value is slightly larger than 2.14 used in Ref. [5]. With our choice the free $\Delta(1232)$ width is 0.118 GeV. The values of axial couplings are standard: $g_A = 1.267$ and $f_\pi = 93$ MeV. We use averaged masses for nucleons and pions: $M = \frac{1}{2}(M_n + M_p)$ and $m_\pi = \frac{1}{3}(m_{\pi^+} + m_{\pi^-} + m_{\pi^0})$ with the values given by the Particle Data Group [21]. For the Δ-resonance contributions we assume $M_\Delta = 1.232$ GeV. In the Delta pole (ΔP) and crossed Delta pole (CΔP) amplitudes $G_{\alpha\beta}(p_\Delta)$ denotes the Rarita-Schwinger (spin-$\frac{3}{2}$ field) propagator. By $\Gamma^{\beta\mu}(p,q)$ we denote the Δ electroweak excitation vertex. We will give more details about the Δ propagator and decay width in the next section. The electroweak excitation vertex as well as the set of vector and axial form factors is described in Appendix D. For the nucleon weak currents present in (13) and (14) we use the standard vector-axial prescription:

$$j^{\mu}_{CCN}(q) = V^\mu(q) - A^\mu(q),$$
$$V^\mu(q) = F_1^V(Q^2)\gamma^\mu + \frac{i}{2M}\sigma^{\mu\alpha}q_\alpha F_V^2(Q^2), \quad (18)$$
$$A^\mu(q) = G^A(Q^2)\left(\gamma^\alpha\gamma^5 + \frac{\not{q}}{m_\pi^2-q^2}q^\alpha\gamma^5\right).$$

From the conserved vector current (CVC) hypothesis one can also get constraints on the form factors of contact term (CT) and pion-in-flight (PIF) diagrams:

$$F_{PIF}(Q^2) = F_{CT}(Q^2) = F_1^V(Q^2). \quad (19)$$

We choose the same nucleon form factors as in Ref. [5]. Details are described in Appendix C. Our current matrix elements contain a virtual pion form factor $F_\pi(k-q)$ coming from the PIF term, where the W boson interacts with a virtual pion with momentum $a = k - q$. The CVC forces one to include it in several other background terms. F_π is assumed to have a monopole form:

$$F_\pi(a) = \frac{\Lambda_\pi^2 - m_\pi^2}{\Lambda_\pi^2 - a^2}; \quad \Lambda_\pi = 1.25\ \text{GeV}. \quad (20)$$

The ρ-meson form factor, having a monopole form $F_\rho(a) = \frac{1}{1-a^2/m_\rho^2}$, with $m_\rho = 0.7758$ GeV, has been introduced in the PP term by the authors of [5] in order to account for the ρ-meson dominance of $\pi\pi NN$ coupling. Because of the partially conserved axial current (PCAC) hypothesis it has been also introduced into the axial part of CT. For each physical pion production channel there is a set of isospin Clebsch-Gordan coefficients C_i listed in Table I. In the carbon

TABLE I. Charged-current isospin coefficients of (11)–(17).

Process	ΔP	CΔP	NP	CNP	Others
$\nu_l + p \to l^- + \pi^+ + p$	$\sqrt{3}$	$\sqrt{\frac{1}{3}}$	0	1	1
$\nu_l + n \to l^- + \pi^0 + p$	$-\sqrt{\frac{2}{3}}$	$\sqrt{\frac{2}{3}}$	$\sqrt{\frac{1}{2}}$	$-\sqrt{\frac{1}{2}}$	$-\sqrt{2}$
$\nu_l + n \to l^- + \pi^+ + n$	$\sqrt{\frac{1}{3}}$	$\sqrt{3}$	1	0	-1
$\overline{\nu}_l + n \to l^+ + \pi^- + n$	$\sqrt{3}$	$\sqrt{\frac{1}{3}}$	0	1	1
$\overline{\nu}_l + p \to l^+ + \pi^0 + n$	$\sqrt{\frac{2}{3}}$	$-\sqrt{\frac{2}{3}}$	$-\sqrt{\frac{1}{2}}$	$\sqrt{\frac{1}{2}}$	$\sqrt{2}$
$\overline{\nu}_l + p \to l^+ + \pi^- + p$	$\sqrt{\frac{1}{3}}$	$\sqrt{3}$	1	0	-1

cross-section computations we sum up contributions from protons and neutrons in an incoherent way.

The Fogli-Nardulli model [3], which in the past was considered as an alternative to the Rein Sehgal [22] model, contains contributions from several background terms: nucleon Born and crossed diagrams and the direct neutrino-pion interaction diagram. However, the CΔP, CT, and PP diagrams are absent, since they appear in a natural way only if one starts from the chiral field theory formalism. In our model we do not include nucleon resonances from the second resonance region and consider neutrino energies $E_\nu \leqslant 1$ GeV. In general, it should be possible to add to the model also heavier resonances. However, these resonances have pole masses above the two-pion-production threshold and there is a significant branching ratio for decay channels with two pions in the final state. Thus consistency would require us to expand the effective field theory Lagrangian to higher order and add the two-pion-production terms as well (see Refs. [23]). One should remember that effective field theory works as long as one can use only tree-level amplitudes; it cannot be extended to high energies. The authors of Refs. [23] constrain predictions from the model to $E_\nu \leqslant 3$ GeV. This is rather unfortunate for experiments with a large fraction of higher energy neutrinos such as MINERvA and LBNE which will probably have to rely on extrapolations from the deep inelastic scattering region justified by the quark-hadron duality hypothesis from Ref. [24].

1. Δ(1232) *decay width and propagator*

The $\pi N\Delta$ interaction is described by the Lagrangian

$$\mathcal{L}_{\pi N\Delta} = \frac{f^*}{m_\pi}\overline{\psi}_\mu \mathbf{T}^\dagger(\partial^\mu\phi)\Psi + \text{H.c.} \tag{21}$$

In the above equation by $\overline{\psi}_\mu$ we denote the Rarita-Schwinger field, by $\phi = (\phi_1, \phi_2, \phi_3)$ we denote the isotriplet of pion fields in Cartesian isospin coordinates, and by Ψ we denote the nucleon field isodoublet. $\mathbf{T}^\dagger$ is the isospin-1/2 to isospin-3/2 transition matrix operator. This results in the following formula for the free vacuum $\Delta \to \pi N$ decay width:

$$\Gamma^{\text{vac}}_{\Delta\to N\pi}(W) = \frac{1}{12\pi}\frac{f^{*2}}{m_\pi^2}\frac{k^3_{cm}(E_{N,cm}+M)}{W}. \tag{22}$$

It is noteworthy that the authors of [19] and [25] use

$$\Gamma^{\text{vac}}_{\Delta\to N\pi}(W) = \frac{1}{12\pi}\frac{f^{*2}}{m_\pi^2}\frac{k^3_{cm}(2M)}{W}. \tag{23}$$

In the above formulas *cm* denotes the Δ center-of-mass frame and W is the hadronic system invariant mass.

The default Δ propagator is given by

$$G^{\alpha\beta}(p_\Delta) = \frac{P^{\alpha\beta}_{3/2}(p_\Delta, M_\Delta)}{p_\Delta^2 - M_\Delta^2 + iM_\Delta\Gamma_\Delta(p_\Delta^2)}, \tag{24}$$

$$P^{\alpha\beta}_{3/2}(p_\Delta, M_\Delta) = -(\not{p}_\Delta + M_\Delta)\Big(g^{\alpha\beta} - \frac{1}{3}\gamma^\alpha\gamma^\beta - \frac{2}{3}\frac{p^\alpha_\Delta p^\beta_\Delta}{M^2_\Delta} + \frac{1}{3}\frac{p^\alpha_\Delta\gamma^\beta - p^\beta_\Delta\gamma^\alpha}{M_\Delta}\Big). \tag{25}$$

$P^{\alpha\beta}_{3/2}$ is the projection operator on spin-$\frac{3}{2}$ states with p_Δ being the Δ resonance four-momentum and Γ_Δ being the free resonance decay width given in Eq. (22).

2. Δ *self-energy*

The Δ(1232) isobar exhibits a strongly medium-dependent behavior due to the possibility of decay into a pion-nucleon pair. The free resonance decay width decreases because of Pauli blocking. By assuming a uniform distribution of decay pions in the Δ rest frame, the Pauli blocking factor is calculated to be [11]

$$F\big(p^0_\Delta, |\mathbf{p}_\Delta|, E_F\big) = \frac{p^0_\Delta E_{N,cm} + |\mathbf{p}_\Delta|k_{cm} - E_F W}{|\mathbf{p}_\Delta|k_{cm}} \tag{26}$$

and thus, for the given Fermi energy E_F,

$$\Gamma^{\text{vac}}(W) \to \tilde{\Gamma} = F\big(p^0_\Delta, |\mathbf{p}_\Delta|, E_F\big)\Gamma^{\text{vac}}(W). \tag{27}$$

Inside the nucleus other decay channels are also opened: two- and three-nucleon absorption channels. The net effect is an overall increase of the Δ width:

$$\begin{aligned}\Gamma^{\text{vac}}_\Delta(W) &\to 2\left(\tfrac{1}{2}\tilde{\Gamma}_\Delta + i\Sigma^{\text{matter}}_\Delta\right)\\ &= \tilde{\Gamma}_\Delta - 2(\Im\Sigma_{1\text{p}1\text{h}1\pi} + \Im\Sigma_{2\text{p}2\text{h}} + \Im\Sigma_{3\text{p}3\text{h}}) + 2i\Re\Sigma_\Delta.\end{aligned} \tag{28}$$

In Ref. [11] Oset parametrized this width as a function of either the incoming pion kinetic energy $x = \frac{T_\pi}{m_\pi}$ or the real photon energy and the local density of nuclear matter. We use his approach in our computations. It is necessary to translate the Oset results obtained in the kinematical situations of real photon or pion scattering to the situation of virtual boson interaction. It was assumed that the functions

$$\begin{aligned}-\Im\Sigma_{1\text{p}1\text{h}1\pi} &= C_{1\text{p}1\text{h}1\pi}\left(\frac{\rho}{\rho_0}\right)^{,\alpha}\\ -\Im\Sigma_{2\text{p}2h} &= C_{2\text{p}2\text{h}}\left(\frac{\rho}{\rho_0}\right)^{\beta},\\ -\Im\Sigma_{3\text{p}3\text{h}} &= C_{3\text{p}3\text{h}}\left(\frac{\rho}{\rho_0}\right)^{\gamma},\\ \rho_0 &= 0.17\ \text{fm}^{-3}\end{aligned} \tag{29}$$

(in which all C_x and α, β, and γ are functions of photon energy or pion kinetic energy) are in a good approximation functions of the average invariant hadronic mass, $\langle W^2\rangle$. The relations

$$\langle W^2\rangle = \begin{cases} M^2 + 2E_\gamma\langle E_N(\rho_N)\rangle, & \gamma,\\ M^2 + 2E_\pi\langle E_N(\rho_N)\rangle + m^2_\pi, & \pi,\end{cases} \tag{30}$$

together with $W^2 = (p_N + q)^2$, allow us to translate the virtual boson into one of the available parametrizations. For the real part of the self-energy we use the same approach as in Refs. [8–10]:

$$\Re(\Sigma) = 40\frac{\rho(r)}{\rho_0}\ \text{MeV}. \tag{31}$$

This prescription neglects different renormalizations of the longitudinal and transverse Δ response functions in the nuclear medium, but for our purpose it is sufficient.

The main problem in using this approach in the model of Ref. [5] comes from the fact that Σ_Δ is calculated using nonperturbative effects not included in tree-level diagrams of Eqs. (11)–(17). All of them contain a single-pion interaction vertex. Thus we modify only the widths in the denominator of the ΔP diagram by substituting

$$\frac{1}{p_\Delta^2 - M_\Delta^2 + iM_\Delta\Gamma^{\rm vac}(W)} \rightarrow \frac{1}{p_\Delta^2 - M_\Delta^2 + iM_\Delta[\tilde{\Gamma} - 2(\Im\Sigma_\Delta - i\Re\Sigma_\Delta)]}. \quad (32)$$

The many-body correction to the SPP through the Δ resonance $\Im\Sigma_{\rm 1p1h1\pi}$ and cross sections for multinucleon channels connected to $\Im\Sigma_{\rm 2p2h}$ and $\Im\Sigma_{\rm 3p3h}$ can be accounted for by replacing the $|\Delta{\rm P}|^2$ contribution (11) by a full Δ resonance production cross section:

$$\frac{d^3\sigma}{dE'd\Omega'} \approx \frac{G_F^2|\mathbf{l}'|}{16\pi^5|\mathbf{l}|}\int drr^2\int d^3p\frac{n_N(p)\left(\frac{1}{2}\tilde{\Gamma} - \Im\Sigma_\Delta\right)}{E(p)(M_\Delta + W)} \times \frac{{\rm Tr}\left[\gamma^0\Gamma^{\alpha\mu^\dagger}\gamma^0 P^{3/2}_{\alpha\beta}(p_\Delta)\Gamma^{\beta\nu}(\not{p} + M)\right]L_{\mu\nu}}{[W - (M_\Delta + \Re\Sigma_\Delta)]^2 + \left(\frac{1}{2}\tilde{\Gamma} - \Im\Sigma_\Delta\right)^2}. \quad (33)$$

The approximation comes from the nonrelativistic expansion in the Δ propagator, $p_\Delta^2 - M_\Delta^2 + iM_\Delta\Gamma_\Delta \approx (M_\Delta + W)(W - M_\Delta + \frac{i}{2}\Gamma_\Delta)$. In the case of electron scattering off protons and neutrons one gets the same isospin factor of 1. In the case of neutrino/antineutrino scattering off protons/neutrons one gets an isospin factor of 3 because of the Clebsch-Gordan coefficient $\sqrt{3}$ in the weak Δ excitation vertex. The decays of the Δ resonance into a pion-nucleon pair are then calculated for different charge states using the Clebsch-Gordan coefficients of $\Delta \rightarrow \pi N$ reactions. The pionless process depends only on the isospins in the primary Δ excitation vertex.

III. NUMERICAL PROCEDURES

The full integration of the cross section within LDA [as given in Eqs. (1) and (2)] even with the assumption of spherically symmetric nuclear matter distribution and on-shell nucleons would require performing six nested integrals. For a small $O(10)$ number of integration points in each of them we would need to evaluate $O(10^6)$ points in the numerical integration procedure to obtain just one point in the triple-differential cross section. Thus the authors of [19] assumed the nucleon momentum to be an average one in a local Fermi sea, $\langle|\mathbf{p}|\rangle = \sqrt{\frac{3}{5}}k_F^N(\mathbf{r})$. Furthermore, $\mathbf{p}$ is assumed to be orthogonal to the $(\mathbf{q}, \mathbf{k})$ plane. Within this approximation the number of nested integrals is reduced by a factor of 2:

$$-\frac{1}{\pi}\Im\left(\Pi^{\mu\nu}_{\rm 1p1h1\pi}L_{\mu\nu}\right) \approx \int\frac{d^3k}{(2\pi)^3}\frac{1}{2E_\pi(k)}{\rm Tr}\left[A^{\mu\nu}_{\rm 1p1h1\pi}(\langle p\rangle, q, k)\right]L_{\mu\nu}$$

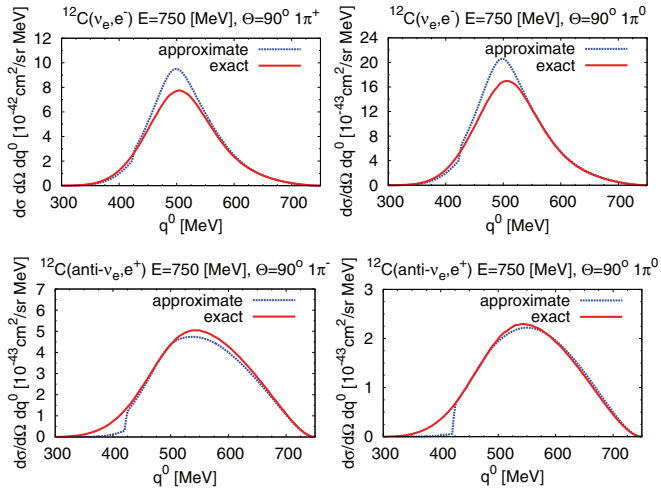

FIG. 2. (Color online) Difference between the exact cross-section calculation from this paper and approximations used in [19].

$$\times\int\frac{d^3p}{(2\pi)^3}\frac{1}{4E(p)E(p')}\{n_N(p)[1 - n_{N'}(p')] + n_{N'}(p')[1 - n_N(p)]\}\delta(E(p') - q^0 + E_\pi - E(p)). \quad (34)$$

The integral over d^3p can now be performed analytically, giving a result proportional to the Lindhard function. There are severe shortcomings of this approximation and we lose some precision. One example is the threshold behavior of the pion production cross section. The hadronic tensor is described by an *averaged* invariant pion-nucleon mass. Thus the physically meaningful tensor is obtained when

$$\langle W^2\rangle = M^2 + 2\langle E_N\rangle q^0 + q_\mu^2 \geqslant (M + m_\pi)^2. \quad (35)$$

The above-mentioned condition is important for the nucleon pole (NP) diagram, for which an unphysical W^2 may give rise to a singularity at $(\langle p\rangle + q)^2 = M^2$. This requires an additional cutoff in the acceptable kinematics, which sometimes moves up the threshold for the pion production process in an artificial way.

However, the six-dimensional integration can be performed using Monte Carlo techniques. There exist several available algorithms for that. We have chosen the Vegas algorithm implemented in the GNU Scientific Library (GSL) for C/C++ compilers [26]. It is efficient enough to perform the eight-dimensional total-cross-section integration in a reasonable time using only $O(10^5)$ points. This solves the threshold problem caused by the averaged hadronic tensor with averaged W^2.

In order to show the difference between the exact calculation and the approximation adopted in Eq. (34) we calculated a sample double-differential electron neutrino cross section off carbon. The results are shown in Fig. 2 for neutrinos (top) and for antineutrinos (bottom). The curves calculated using Eq. (34) are quite different from those calculated without approximations.

For the total cross section both the exact and approximate approaches give similar results, as one can see in Fig. 3. In the case of antineutrino charged pion production there is a

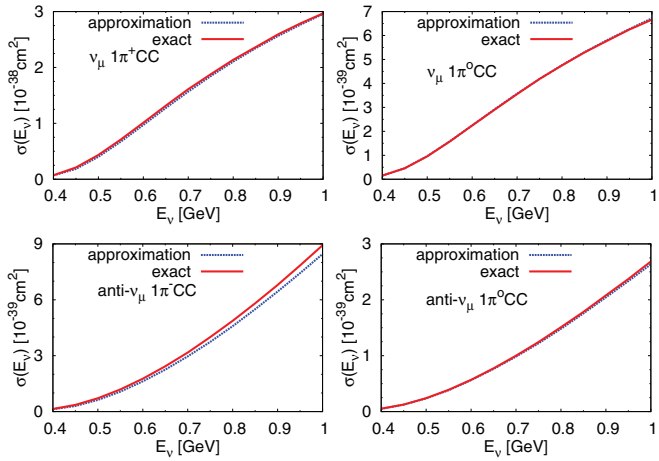

FIG. 3. (Color online) Difference between the exact cross-section calculation from this paper and approximations used in [19].

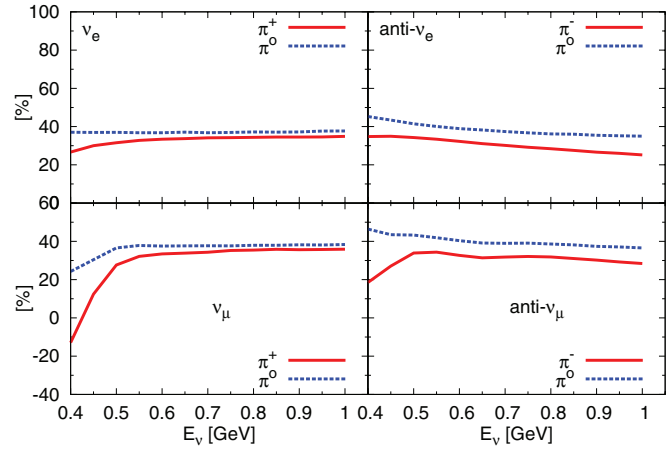

FIG. 5. (Color online) Impact of nuclear effects on SPP off ^{12}C. Plots show $(\sigma_{\text{free}} - \sigma_{\text{medium}})/\sigma_{\text{free}} \times 100\%$.

systematic difference between our calculation and approximated results, but it is rather small. Thus we find the approximation given by Eq. (34) sufficient on the level of total cross sections. In what follows we will always rely on the exact calculations.

IV. RESULTS

A. Importance of background terms

Figure 4 shows the importance of background terms for pion production on a set of six free protons and six free neutrons. The curves describe ratios of cross sections coming from only the Delta pole diagram to the cross section calculated with all the background diagrams (and the interference terms) included in computations.

We see that, especially for low neutrino energies, below 500 MeV, the background contribution is very important. The background terms are more relevant for antineutrinos than for neutrinos and for π^0 production than for charged pion production.

B. Importance of in-medium effects

Figure 5 shows the impact of in-medium effects on pion production. We plotted a relative modification of the free

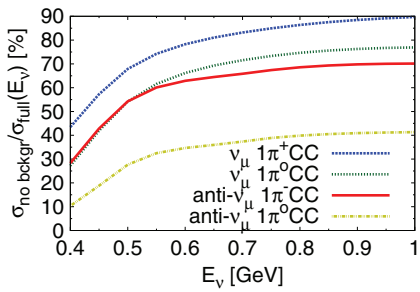

FIG. 4. (Color online) Ratios of the total cross sections for ν_μ and $\bar{\nu}_\mu$ SPP reactions on carbon calculated with a model without the background terms to the predictions of the full model of this paper.

nucleon cross section (six free protons and neutrons but with the background contribution included) caused by in-medium effects. In almost all of the cases in-medium effects lead to a significant decrease of the total cross section. For the electron (anti)neutrinos, where energy 400 MeV is far from the SPP reaction threshold, we see an almost constant reduction of the cross section on the level of 30%–40%. There is an interesting difference in shapes between the curves for electron neutrinos and antineutrinos (see Fig. 5). The latter exhibits a smooth drop of in-medium reduction with growing neutrino energy. In the case of muon neutrinos and antineutrinos near the pion production threshold ($E_\nu < 0.5$ GeV) the cross section is less affected by nuclear effects. For the π^+ production channel and $E_\nu = 0.4$ GeV it even seems to be slightly enhanced. This happens due to the nucleon Fermi motion, which dominates other effects in that kinematical region. This is not the case for π^0 production by antineutrinos. There exists a correlation between the nonresonant background contribution and the cross-section reduction due to in-medium effects. The shapes of the reduction ratios in neutrino π^0 and antineutrino π^- channels are almost the same, so is the background contribution shown in Fig. 4. In general, the more the cross section comes from background and interference terms, the smaller is the near-threshold effect. For higher muon neutrino and antineutrino energies, $E > 0.6$ GeV, we see again an almost uniform reduction of the cross section of the order of 30%.

Similar studies were done in [10], where a LFG-based model of a carbon nucleus has been used with the same parametrization of Δ self-energy, but without nonresonant terms. In [27] a global relativistic Fermi gas (RFG) and a relativistic plane-wave impulse approximation (RPWIA) with realistic bound-state wave functions calculated within the Walecka σ-ω model were studied. For medium modifications of the Δ resonance the global density $\rho = 0.75\rho_0$ is applied, leading to a constant increase in the Δ mass and self-energy estimated to be 30 and 40 MeV, correspondingly. Within the Δ dominance model the calculations were performed for carbon and iron targets and muon neutrinos. RFG and RPWIA models lead to very similar results. Without the Δ

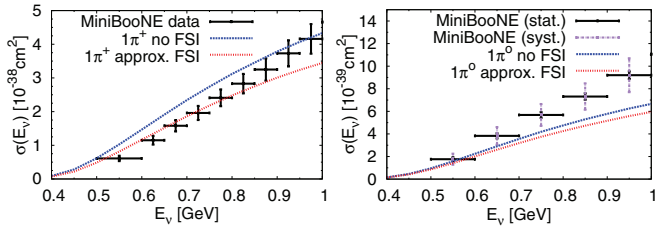

FIG. 6. (Color online) Charged and neutral pion production cross sections on CH_2 for the full model of this paper. The data are taken from Refs. [17] and [18].

in-medium effects, RFG and RPWIA total SPP cross sections are reduced by 50% or more at 400 MeV and by about 15% at 1 GeV with respect to the free-proton cross section. There seems to be no near-threshold cross-section enhancement due to the Fermi motion. The Δ in-medium effects (in the adopted approximation of the constant nuclear density) lead to a further reduction of SPP cross section in carbon (about 45% at $E_\nu = 800$ MeV).

C. Total cross sections

We compared predictions from our model with the recent MiniBooNE pion production data. The MiniBooNE Collaboration, unlike the K2K Collaboration, published its results in the form of absolutely normalized cross section and not as a ratio to CC inclusive cross sections. We performed calculations with our model of the total SPP cross sections on CH_2. A direct comparison with the data is not straightforward because the MiniBooNE Collaboration reported the cross sections for pions in the final state after leaving the nucleus (in a case of neutrino-carbon scattering) with all the FSI effects included. The pion FSI effects can be evaluated within a cascade model like those implemented in Monte Carlo event generators. Our model is not yet an ingredient of any MC generator and we decided to estimate the impact of FSI effects using the results of a MC comparison study published in Ref. [28]. We approximate the relevant probabilities as

$$P(\pi^0 \to \pi^0) = 67\%, \quad P(\pi^0 \to \pi^+) = 5\%, \tag{36}$$

$$P(\pi^+ \to \pi^+) = 69\%, \quad P(\pi^+ \to \pi^0) = 5\%. \tag{37}$$

The results for the cross section with and without FSI are plotted in Fig. 6.

For charged pion production we obtained a quite good agreement with the data up to the neutrino energy of around 0.8 GeV. In the case of charged-current π^0 production both free and in-medium cross sections calculated with our model are too small, and the discrepancy becomes larger with increasing neutrino energy. FSI introduce large modifications for the π^+ channel. In the π^0 channel the effect of absorption of π^0 is partially compensated for by a fraction of initial π^+ events, which end up as π^0 due to the charge exchange reaction inside the nucleus.

The MiniBooNE SPP data were also analyzed by the Giessen group using GIBUU (a code for hadron transport in nuclear matter based on the semiclassical Boltzmann-Uehling-Uhlenbeck equation [29]). The Giessen SPP model covers a larger kinematical region and includes contributions from heavier resonances. In its most recent version the model uses both ANL and BNL data fit to Δ excitation transition form factors and treats them as lower and upper bounds for SPP [30]. The nonresonant background is included in a phenomenological fashion and the pion production cross section is an incoherent sum of two contributions:

$$d\sigma_{SPP} = d\sigma_{\text{res}} + d\sigma_{\text{nonres}}, \tag{38}$$

where the first one comes from the excitation of resonances with invariant masses $W < 2$ GeV and the second one from a nonresonant background and resonance-background interference terms. The vector part of the background is found as a fit to the difference between experimental and theoretical resonant contributions to electron SPP on nucleons. The axial and axial-vector part of the background are assumed to have the same functional form and are scaled by a constant factor in order to get an agreement with the low-energy SPP data. Nuclear effects include a momentum-dependent potential for initial-state nucleons and spectral functions for final-state hadrons (including resonances). The Δ spectral functions include the same in-medium effects as those incorporated in the model discussed in this paper.

Figure 12 from Ref. [30] allows for a comparison with the impact of consecutive nuclear effects on the pion production rate. Fermi motion and Pauli blocking make the Δh excitation cross section smaller by $\sim$5%. A further 5%–8% reduction of the cross section is introduced by Δ self-energy. Finally, due to pionless decay modes, pion production is reduced by an extra 15%–20%. In Ref. [30] predictions for SPP cross sections for energies up to 2 GeV are shown and it is clearly seen that in the range discussed in this paper ($E_\nu \leqslant 1$ GeV) the contribution from heavier resonances is negligible.

Interesting are comparisons of the GiBUU model with the MiniBooNE CC pion production data. For π^+ production the computations based on BNL-fitted form factors are slightly below the data (including error bars) and the difference is largest at neutrino energies of 1–1.5 GeV. In the case of π^0 production the situation is slightly better and except for the region of about 1 GeV the predictions agree with the data, again including error bars. ANL-fitted form factors produce predictions which fall far apart from the MiniBooNE data points.

A good review of the discrepancies between different theoretical SPP calculations and experimental data (as well as of other types of neutrino-nucleus interactions) can be found in Ref. [2].

D. Ratios of muon to electron (anti)neutrino cross sections

In neutrino oscillation appearance experiments it is very important to calculate precisely the ratios of muon and electron neutrino cross sections. Even in the presence of a near detector and with full understanding of the initial muon neutrino flux a good knowledge of the ratios (and their dependence on the neutrino energy) is crucial for the correct identification of the oscillation signal.

In Fig. 7 we see that the ratios calculated with the complete model are slowly increasing functions of the neutrino energy.

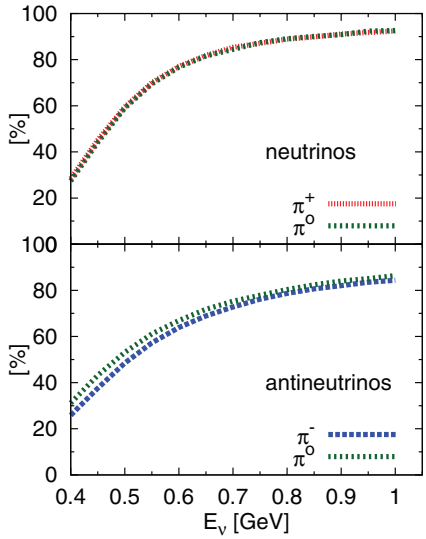

FIG. 7. (Color online) Ratios of muon to electron (anti)neutrino total SPP cross sections on ^{12}C for the full model of this paper.

In the case of antineutrinos there is a small difference between π^- and π^0 production: in the first case the ratio is slightly lower. In contrast, we obtain almost the same ratios for π^+ and π^0 production by neutrinos.

It is important to know how well the ratios are calculated when simpler models of SPP are used, which is often the case in MC event generators.

Figure 8 shows the impact of the background terms on π^0 production ratios. We compared two situations: the full model and the model without background contributions. We see that the results are significantly different only in the case of antineutrinos. For lower neutrino energies using a purely resonant SPP mechanism one obtains much smaller ratios. For the neutrinos these differences are negligible. The resonant

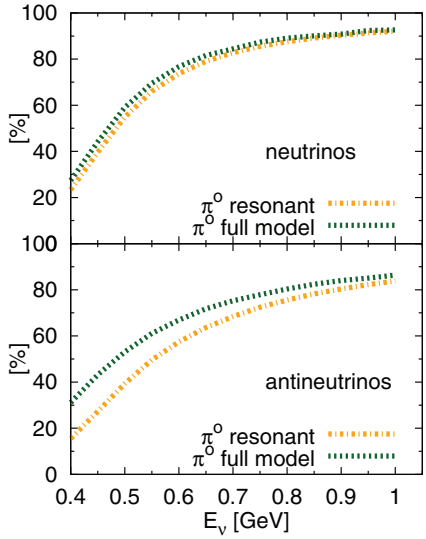

FIG. 8. (Color online) Ratios of muon to electron (anti)neutrino total SPP cross sections on ^{12}C for the full model of this paper and for the resonant SPP only (without the background terms).

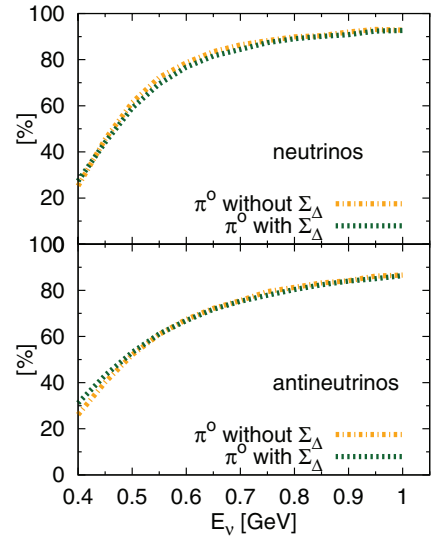

FIG. 9. (Color online) Ratios of muon to electron (anti)neutrino total SPP cross sections on ^{12}C for the full model of this paper with and without the Δ self-energy Σ_Δ.

contribution ratio is very close to the one plotted in Ref. [8] for the sum of neutrino and antineutrino cross sections in a similar model.

Figure 9 shows the effect of the Δ self-energy on the ratios. We compared two situations: the full model and the model without the Δ self-energy. We see that neglecting the Δ self-energy has almost no effect on the considered observable. We conclude that in order to evaluate well the antimuon to antielectron neutrino cross-section ratio it is important to include the nonresonant background, but not necessarily the Δ self-energy.

We also investigated the possible impact on predictions from the model coming from alternative descriptions of the Δ resonance vacuum width. For example, the authors of Ref. [31] use

$$\Gamma^{\text{vac}}_{\text{M-S}}(W) = 118\ \text{MeV} \cdot \frac{\rho_{\Delta\to\pi N}(W)}{\rho_{\Delta\to\pi N}(M_\Delta)},$$
$$\rho_{\Delta\to\pi N}(W) = \frac{k_{cm}}{W}\frac{k_{cm}^2 R^2}{1+k_{cm}^2 R^2}, \quad R = 1\ \text{fm}. \tag{39}$$

The term $\frac{k_{cm}^2 R^2}{1+k_{cm}^2 R^2}$ is the so-called Blatt-Weisskopf centrifugal barrier. In this manner one accounts for phenomenological knowledge of the decay πN system angular momentum, which is absent in the Lagrangian given in Eq. (21). Furthermore, one can account partially for the off-shell Δ effects by replacing the propagator in the ΔP term [Eq. (24)] by

$$\tilde{G}^{\alpha\beta}(p_\Delta) = \frac{\tilde{P}^{\alpha\beta}_{3/2}(p_\Delta)}{p_\Delta^2 - M_\Delta^2 + iW\Gamma_\Delta(p_\Delta^2)}$$
$$= -\frac{(\not{p}_\Delta + W)}{p_\Delta^2 - M_\Delta^2 + iW\Gamma_\Delta(p_\Delta^2)}\left(g^{\alpha\beta} - \frac{1}{3}\gamma^\alpha\gamma^\beta - \frac{2}{3}\frac{p_\Delta^\alpha p_\Delta^\beta}{W^2} + \frac{1}{3}\frac{p_\Delta^\alpha\gamma^\beta - p_\Delta^\beta\gamma^\alpha}{W}\right). \tag{40}$$

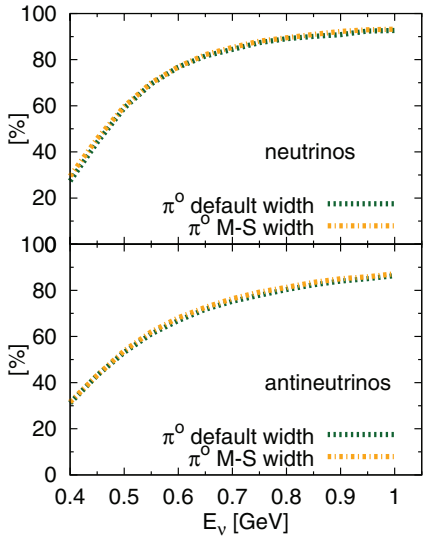

FIG. 10. (Color online) Ratios of muon to electron (anti)neutrino total SPP cross sections on ^{12}C for the full model of this paper with the Δ width described by Eqs. (22) and (39).

This convention is used in Ref. [32] together with the Manley-Saleski decay width from Ref. [31]. Thus whenever we use Eq. (39) we also replace Eq. (24) by Eq. (40). In order to be consistent, after changing the width (22) with (39) in (40) one also has to multiply the whole expression by $\sqrt{\frac{\Gamma^{\rm vac}_{\rm M\text{-}S}(W)}{\Gamma^{\rm vac}_{\Delta}(W)}}$. This compensates for the fact that our current has a decay vertex defined by (21) in the numerator, which leads to the width (22).

On the level of total cross sections the difference between two $\Delta\pi N$ decay descriptions is negligible. This is illustrated in Fig. 10, where we plot again the muon to electron (anti)neutrino total π^0 production cross-section ratios and we compare the default and the Manley-Saleski Δ description.

In the work of Barbero *et al.* [7] the nonresonant background is described in a way quite similar to that used in Ref. [5] (where ρ and ω meson diagrams were used instead of the PP contribution). The authors of [7] have pointed out that the standard Rarita-Schwinger spin-3/2 projection operator used in Eqs. (24) and (40) should be replaced by a more consistent approach. In this treatment one demands invariance under the contact transformations of Rarita-Schwinger fields, eliminating the spurious spin-1/2 degree of freedom in the on-shell Rarita-Schwinger propagator. One can then introduce a set of *reduced* Feynman rules [33], which include a *reduced* Δ propagator, different from Eqs. (24) and (40). The effect of switching between the reduced and Rarita-Schwinger propagators on the pion production in a model containing nonresonant background can be as large as 30% (depending on the pion production channel). Using a reduced Δ propagator leads to a better agreement with ANL and BNL data in Ref. [7] than in Ref. [5]. It is worth mentioning that using the reduced propagator has a significant impact only in models containing background terms. In Ref. [27] similar changes to the Δ propagator following Pascalutsa [34] have been made in a Δ-dominance model, leading to negligible changes in the resonant SPP.

Finally, we investigated also how much the numerical approximation in Eq. (34) affects the muon to electron neutrino cross-section ratios. This is illustrated in Fig. 11, where we have plotted $\overline{\nu}_\mu/\overline{\nu}_e$ $1\pi^0$CC cross-section ratios. Differences are present only for energies $E_\nu < 550$ MeV, and at $E_\nu = 500$ MeV it is about 4%.

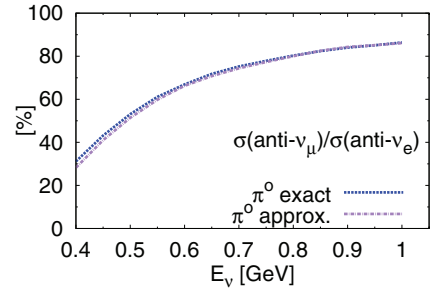

FIG. 11. (Color online) Ratios of $\overline{\nu}_\mu$ to $\overline{\nu}_e$ neutrino CCπ^0 SPP cross sections on ^{12}C calculated with the full model of this paper and with approximations used in Ref. [5].

E. Pionless Δ decays

An interesting feature of our model is that there exists a contribution to the cross section coming from pionless Δ decays. This is a part of the meson exchange current (MEC) cross section, which has recently attracted a lot of attention [1]. There is a lot of evidence that the MEC mechanism is responsible for a large CCQE axial mass measurement reported by the MiniBooNE Collaboration [35]. Theoretical microscopic computations always include pionless Δ decays as part of the calculated effect. In some MC event generators (e.g., NEUT and NUANCE) a constant fraction of the pionless Δ decays is assumed and we find it interesting to check how well this assumption is satisfied in our model.

The fractions of pionless decays and their dependence on neutrino energy and species are shown in Fig. 12. There is no difference between neutrinos and antineutrinos, because we include only the npnh mechanism coming from the resonant diagrams. The fraction of pionless Δ decays is very large for energies below 500 MeV. For higher energies it exhibits a smooth energy dependence, dropping down to 20% at $E_\nu = 1$ GeV. It is clear that for experiments with a large fraction of neutrinos with energies below 1 GeV one cannot consider the investigated quantity to be constant.

The total pionless Δ decay cross section may be treated as a lower bound for the npnh contribution. One has to keep in mind

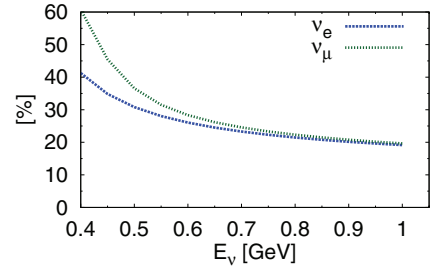

FIG. 12. (Color online) Fraction of the pionless Δ decays to the resonant SPP production cross section $(\sigma_{\text{pionless }\Delta})/\sigma_{\text{SPP res.}} \times 100\%$ in ^{12}C for ν_e and ν_μ.

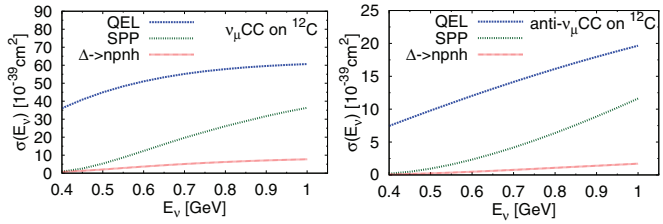

FIG. 13. (Color online) Total CC cross sections on ^{12}C for quasielastic scattering, SPP, and pionless Δ decay.

that there are many other sources of npnh final states which can be built from diagrams in Fig. 1 but are not considered in this paper. The total cross section coming from $\Delta \to npn$h decays can be seen in Fig. 13. The charged-current quasielastic contribution has been calculated with the NuWro neutrino event generator [36] within the spectral function (SF) approach [37] and with $M_A = 1.05$ GeV. The npnh contribution coming from pionless Δ decays may seem small compared to CCQE and SPP cross sections (around 10%–15% of the first), but at $E_\nu = 1$ GeV it accounts for about 60% of the npnh cross section in the model of Nieves *et al.* [19] (and at $E_\nu =$ 750 MeV the fraction is even larger and amounts to 64%).

V. CONCLUSIONS AND OUTLOOK

We have investigated in detail the model of single-pion production on nuclei based on effective field theory. The nuclear model includes local Fermi gas effects, Pauli blocking, and Δ in-medium self-energy. Contributions from heavier resonances are neglected; thus the model is expected to reproduce well the data in the energy region $E_\nu \leqslant 1$ GeV. We use an open-source MC integration algorithm, which allows us to avoid many numerical approximations present in Ref. [19].

We have analyzed in detail the ratio of muon to electron neutrino cross sections for pion production because this is an important theoretical input in neutrino oscillation appearance experiments. The inclusion of nonresonant background has a non-negligible impact on the analyzed observables. It is more pronounced in the antineutrino channels, where the background terms play a major role in the considered neutrino energy region. The muon to electron neutrino cross-section ratios for neutrinos do not depend on the final-state pion charge, whereas for the antineutrinos we predict a small splitting between the π^- and π^0 channels. This splitting seems to originate from the nonresonant background terms, which give rise to a large fraction of cross section in the antineutrino π^0 production modes (and sometimes the cross section is more than doubled by including the background terms!). We showed that these ratios are almost independent of nuclear effect modeling details such as the self-energy of the Δ resonance or numerical integration approximations proposed in Ref. [19], nor do they depend on the Δ free decay width model changes between the one resulting from the relativistic decay width, Eq. (22), to the one used in the Manley-Saleski analysis, Eq. (39), which incorporates the angular momentum of the decaying hadronic system.

We have also found that one cannot treat the pionless Δ decay fraction as a constant number for neutrino interactions below 1 GeV. This is important, since pionless Δ decay seems to give rise to more than half of the $2p2h$ cross section.

Using an estimate of FSI effects based on [28], we obtained a reasonable agreement with the MiniBooNE CCπ^+ production data but the model underestimates the CCπ^0 cross section. The same problems appear in most of the aforementioned theoretical models and it is likely that something important is missing. Perhaps one needs a better description of the Δ resonance (see, e.g., Refs. [7] and [34], which focus on a more consistent treatment of the Δ propagator). One should also try to investigate other models of nonresonant background (e.g., Ref. [7], because Ref. [5] does not seem to reproduce all isospin channels equally well). This is pronounced in the $\nu_\mu n \to \mu^- p\pi^0$ channel.

In our model the in-medium Δ spectral function was included only in the ΔP diagram and the pure background contribution [36 out of 49 combinations from Eqs. (11)–(17)] is not affected by the presence of nuclear matter. In the Δ-background interference terms (12 combinations) in-medium effects enter only through the ΔP diagram and thus are included only partially. A conclusive verification of the model predictions can be done only by evaluating the nonperturbative in-medium effects for all the genuine amplitudes (28 independent terms). This is a very difficult task to achieve. Because of that we are unable to conclude whether the resulting reduction of the cross section is a genuine physical effect or rather an artifact of the adopted approximations.

Another possible explanation for the existing disagreement with the data is that there is a large $1\pi 2p2h$ contribution (analogous to the 2p2h-enhancing CCQE-like cross section) neglected in the computations. In Ref. [30] there is an interesting comment that the comparison of data to theoretical computations for pion photoproduction on carbon suggests that the data are underestimated (at $E_\gamma = 500$ MeV by around 20%) and a possible explanation is the neglected $1\pi 2p2h$ contribution.

All the consistent $2p2h$ models are constructed based on SPP diagrams with virtual pions connected to nucleons. Thus it seems crucial to have a good SPP model in order to build also a consistent two-nucleon current theory and estimate the multinucleon knock-out contamination of CCQE-like data samples.

ACKNOWLEDGMENTS

J.Ż. would like to thank L. Alvarez-Ruso, K. Graczyk, and J. Nieves for many fruitful discussions. This work was sponsored by Grants No. 4525/PB/IFT/11 (UMO-2011/01/N/ST2/03224) and No. 4574/PB/IFT/12 (UMO-2011/01/M/ST2/02578).

APPENDIX A: NOTATION AND CONVENTIONS

We adopt the conventions from Bjorken-Drell [$g^{\mu\nu} =$ $(+,-,-,-)$ etc.], the only difference being in the Dirac spinor

normalization

$$\sum_s u_s(\boldsymbol{p})\overline{u}_s(\boldsymbol{p}) = \not{p} + m, \tag{A1}$$

which is convenient for our calculations.

APPENDIX B: NUCLEAR MATTER DENSITY PARAMETRIZATION

We took the harmonic oscillator density profiles from [38]:

$$\rho(\mathbf{r}) = \rho_0[1 + a(r/R)^2]\exp[-(r/R)^2], \tag{B1}$$

with corrections to parameters a and R calculated in [39]. These parameters are slightly different for protons and neutrons. The local Fermi momentum is calculated from the relation $k_F^N(\mathbf{r}) = [3\pi^2\rho(\mathbf{r})^N]^{\frac{1}{3}}$. The authors of Ref. [19] subtract the Fermi kinetic energy from the nucleons inside the medium : $E(p) \to E(p) - T_F$. In this manner they account for the binding effects.

APPENDIX C: NUCLEON FORM FACTORS

The isospin symmetry relates the vector form factors to the electromagnetic ones:

$$F_i^V(Q^2) = F_i^p(Q^2) - F_i^n(Q^2). \tag{C1}$$

For the electromagnetic form factors we use the parametrization of Galster *et al.* [40]:

$$\begin{aligned} F_1^N(Q^2) &= \frac{G_E^N(Q^2) + \tau G_M^N(Q^2)}{1+\tau}, \\ F_2^N(Q^2) &= \frac{G_M^N(Q^2) - G_E^N(Q^2)}{1+\tau}, \\ G_E^p(Q^2) &= \frac{G_M^p(Q^2)}{\mu_p} = \frac{G_M^n(Q^2)}{\mu_n} \\ &= -(1+\lambda_n\tau)\frac{G_E^n(Q^2)}{\mu_n\tau} = \frac{1}{\left(1+\frac{Q^2}{M_D^2}\right)^2}, \end{aligned} \tag{C2}$$

with $\mu_p = 2.792.847$, $\mu_n = 1.913043$, $\lambda_n = 5.6$, $\tau = \frac{Q^2}{4M^2}$, and $M_D = 0.843$ GeV. We assume the axial nucleon form

TABLE II. Total cross sections for $^{12}\mathrm{C}(\nu_e, e^-)$ scattering.

E (GeV)	$\sigma_{6p+6n}(E)$ (10^{-38} cm^2)				$\sigma_{\mathrm{FM+PB}}(E)$ (10^{-38} cm^2)			
	Resonance		+Background		Resonance		+Background	
	π^+	π^0	π^+	π^0	π^+	π^0	π^+	π^0
0.40	0.227	0.045	0.344	0.089	0.315	0.063	0.418	0.090
0.45	0.480	0.096	0.667	0.165	0.606	0.121	0.764	0.164
0.50	0.812	0.162	1.067	0.257	0.960	0.192	1.166	0.251
0.55	1.198	0.240	1.512	0.358	1.346	0.269	1.588	0.343
0.60	1.611	0.322	1.973	0.462	1.745	0.349	2.010	0.435
0.65	2.031	0.406	2.428	0.566	2.133	0.427	2.419	0.522
0.70	2.443	0.489	2.866	0.666	2.511	0.502	2.785	0.605
0.75	2.838	0.568	3.279	0.760	2.862	0.572	3.152	0.682
0.80	3.210	0.642	3.663	0.850	3.182	0.636	3.455	0.750
0.85	3.557	0.711	4.020	0.934	3.478	0.696	3.741	0.817
0.90	3.877	0.775	4.348	1.012	3.743	0.749	3.998	0.876
0.95	4.170	0.834	4.651	1.085	3.988	0.798	4.251	0.927
1.00	4.439	0.888	4.932	1.154	4.218	0.844	4.482	0.983

E (GeV)	$\sigma_{\Delta\text{ in-medium}}(E)$ (10^{-38} cm^2)				$\Delta_{\mathrm{pionless}}$
	Resonance		+Background		
	π^+	π^0	π^+	π^0	
0.40	0.167	0.033	0.251	0.055	0.141
0.45	0.331	0.066	0.467	0.103	0.213
0.50	0.543	0.109	0.731	0.162	0.290
0.55	0.787	0.157	1.017	0.225	0.368
0.60	1.048	0.210	1.313	0.292	0.443
0.65	1.314	0.263	1.610	0.356	0.512
0.70	1.576	0.315	1.888	0.420	0.574
0.75	1.828	0.366	2.156	0.479	0.630
0.80	2.067	0.413	2.405	0.534	0.678
0.85	2.289	0.458	2.632	0.587	0.720
0.90	2.496	0.499	2.847	0.636	0.756
0.95	2.686	0.537	3.042	0.676	0.787
1.00	2.861	0.572	3.212	0.719	0.813

factor to be in a dipole form:

$$G_A(Q^2) = \frac{g_A}{\left(1+\frac{Q^2}{M_A^2}\right)^2}, \quad M_A = 1.05\ \text{GeV}, \qquad \text{(C3)}$$

with $g_A = 1.267$.

APPENDIX D: Δ(1232) FORM FACTORS

The most general electroweak Δ excitation vertex is given by

$$\begin{aligned}\Gamma^{\alpha\mu}(p,q) = \left[V^{\alpha\mu}_{3/2} - A^{\alpha\mu}_{3/2}\right] = \Bigg[&\frac{C_3^V(Q^2)}{M}(g^{\alpha\mu}\not{q} - q^\alpha\gamma^\mu) \\ &+ \frac{C_4^V(Q^2)}{M^2}[g^{\alpha\mu}q\cdot(p+q) - q^\alpha(p+q)^\mu] \\ &+ \frac{C_5^V(Q^2)}{M^2}(g^{\alpha\mu}q\cdot p - q^\alpha p^\mu) + g^{\alpha\mu}C_6^V(Q^2)\Bigg]\gamma^5 \\ &+ \Bigg[\frac{C_3^A(Q^2)}{M}(g^{\alpha\mu}\not{q} - q^\alpha\gamma^\mu) \\ &+ \frac{C_4^A(Q^2)}{M^2}[g^{\alpha\mu}q\cdot(p+q) - q^\alpha(p+q)^\mu] \\ &+ C_5^A(Q^2)g^{\alpha\mu} + \frac{C_6^A(Q^2)}{M^2}q^\alpha q^\mu\Bigg]. \qquad \text{(D1)}\end{aligned}$$

The $C_i^V(Q^2)$ and $C_i^A(Q^2)$ vector and axial form factors determine the $W^\pm N\Delta$ transition. There exist several phenomenological parametrizations of Δ(1232) form factors (see, for example, [8], [9], [10], and [41]). For the vector form factor set we have chosen the parametrization of [20]:

$$\begin{aligned}C_3^V(Q^2) &= \frac{2.13}{\left(1+Q^2/M_V^2\right)^2}\frac{1}{1+Q^2/4M_V^2}, \\ C_4^V(Q^2) &= \frac{-1.51}{\left(1+Q^2/M_V^2\right)^2}\frac{1}{1+Q^2/4M_V^2}, \qquad \text{(D2)} \\ C_5^V(Q^2) &= \frac{0.48}{\left(1+Q^2/M_V^2\right)^2}\frac{1}{1+Q^2/0.776M_V^2},\end{aligned}$$

TABLE III. Total cross sections for $^{12}\text{C}(\overline{\nu}_e, e^+)$ scattering.

E (GeV)	$\sigma_{6p+6n}(E)$ (10^{-38} cm^2)				$\sigma_{\text{FM+PB}}(E)$ (10^{-38} cm^2)			
	Resonance		+Background		Resonance		+Background	
	π^-	π^0	π^-	π^0	π^-	π^0	π^-	π^0
0.40	0.048	0.010	0.084	0.030	0.055	0.011	0.084	0.022
0.45	0.091	0.018	0.148	0.052	0.102	0.020	0.147	0.039
0.50	0.146	0.029	0.225	0.077	0.160	0.032	0.223	0.061
0.55	0.209	0.042	0.312	0.107	0.225	0.045	0.307	0.084
0.60	0.279	0.056	0.408	0.139	0.299	0.060	0.399	0.111
0.65	0.354	0.071	0.512	0.174	0.376	0.075	0.500	0.139
0.70	0.435	0.087	0.623	0.212	0.463	0.093	0.608	0.171
0.75	0.521	0.104	0.741	0.252	0.552	0.110	0.721	0.200
0.80	0.610	0.122	0.865	0.294	0.642	0.128	0.839	0.235
0.85	0.703	0.141	0.994	0.338	0.739	0.148	0.963	0.269
0.90	0.798	0.160	1.129	0.383	0.836	0.167	1.096	0.306
0.95	0.896	0.179	1.270	0.430	0.934	0.187	1.231	0.341
1.00	0.995	0.199	1.415	0.478	1.038	0.208	1.365	0.380

E (GeV)	$\sigma_{\Delta\text{ in-medium}}(E)$ (10^{-38} cm^2)				Δ_{pionless}
	Resonance		+Background		
	π^-	π^0	π^-	π^0	
0.40	0.029	0.006	0.055	0.017	0.022
0.45	0.055	0.011	0.096	0.029	0.032
0.50	0.089	0.018	0.147	0.045	0.044
0.55	0.130	0.026	0.208	0.064	0.057
0.60	0.178	0.036	0.277	0.085	0.071
0.65	0.231	0.046	0.353	0.108	0.086
0.70	0.289	0.058	0.435	0.133	0.101
0.75	0.352	0.070	0.525	0.159	0.116
0.80	0.419	0.084	0.619	0.188	0.132
0.85	0.489	0.098	0.721	0.216	0.147
0.90	0.561	0.112	0.828	0.247	0.162
0.95	0.636	0.127	0.940	0.279	0.177
1.00	0.712	0.142	1.058	0.310	0.192

with $M_V = 0.84$ GeV. The CVC implies that $C_6^V = 0$. The axial part is dominated by the C_5^A contribution. We use the dipole approximation, in which

$$C_5^A(Q^2) = \frac{C_5^A(0)}{\left(1 + Q^2/M_{A\Delta}^2\right)^2}. \tag{D3}$$

We use a default value of the Δ axial mass, $M_{A\Delta} = 1.05$ GeV. The default value of $C_5^A(0)$ is obtained from the Goldberger-Treiman relations [42]:

$$C_5^A(0) = \sqrt{\frac{2}{3}}\frac{f_\pi}{m_\pi} f^* \approx 1.2, \tag{D4}$$

which is somewhat higher than what is used in [5]: $C_5^A(0) \approx 1.15$. The authors of [20] and [5] use $C_5^A(Q^2) = \frac{C_5^A(0)}{(1+Q^2/M_{A\Delta}^2)^2}\frac{1}{1+Q^2/3M_{A\Delta}^2}$. Because of big uncertainties in the axial $N\Delta$ transition, which do not allow one to extract any beyond-dipole behavior, we use the simple dipole form (D3). We include Adler's [43] relation for C_4^A, i.e.,

$$C_4^A(Q^2) = -\tfrac{1}{4}C_5^A(Q^2). \tag{D5}$$

Furthermore, from the PCAC hypothesis one can determine

$$C_6^A(Q^2) = \frac{M^2}{m_\pi^2 + Q^2}C_5^A(Q^2). \tag{D6}$$

The C_3^A form factor is considered to be negligibly small; thus we set $C_3^A(Q^2) = 0$

APPENDIX E: TOTAL CROSS SECTION TABLES FOR ^{12}C

In this Appendix we show our results for different neutrino flavors scattering off ^{12}C (Tables II–V). Cross sections are divided according to the final pion isospin channels and nuclear target modeling starting from free nucleons ($6p + 6n$), through Fermi motion and Pauli blocking effects (FM + PB), up to full medium effects considered in this paper (Δ in-medium). We give the results both for the full model and resonant SPP contribution only. All of the results are given in units of 10^{-38} cm^2.

TABLE IV. Total cross sections for ^{12}C(ν_μ, μ^-) scattering.

E (GeV)	$\sigma_{6p+6n}(E_\nu)$ (10^{-38} cm^2)				$\sigma_{\text{FM+PB}}(E_\nu)$ (10^{-38} cm^2)			
	Resonance		+Background		Resonance		+Background	
	π^+	π^0	π^+	π^0	π^+	π^0	π^+	π^0
0.40	0.028	0.006	0.063	0.020	0.068	0.014	0.110	0.024
0.45	0.138	0.028	0.241	0.066	0.253	0.051	0.354	0.076
0.50	0.408	0.082	0.601	0.151	0.558	0.112	0.723	0.155
0.55	0.779	0.156	1.050	0.253	0.933	0.187	1.148	0.248
0.60	1.189	0.238	1.520	0.359	1.337	0.267	1.594	0.342
0.65	1.613	0.323	1.990	0.466	1.742	0.348	2.012	0.435
0.70	2.041	0.408	2.453	0.570	2.131	0.426	2.419	0.523
0.75	2.463	0.493	2.900	0.672	2.498	0.500	2.786	0.602
0.80	2.859	0.572	3.310	0.766	2.839	0.568	3.116	0.675
0.85	3.226	0.645	3.686	0.853	3.152	0.630	3.436	0.738
0.90	3.564	0.713	4.029	0.935	3.438	0.688	3.690	0.805
0.95	3.873	0.775	4.343	1.010	3.695	0.739	3.957	0.862
1.00	4.155	0.831	4.631	1.080	3.924	0.785	4.186	0.911

E (GeV)	$\sigma_{\Delta\text{ in-medium}}(E)$ (10^{-38} cm^2)				
	Resonance		+Background		Δ_{pionless}
	π^+	π^0	π^+	π^0	
0.40	0.039	0.008	0.072	0.016	0.072
0.45	0.132	0.026	0.211	0.045	0.132
0.50	0.298	0.060	0.435	0.096	0.206
0.55	0.520	0.104	0.713	0.157	0.287
0.60	0.772	0.154	1.011	0.223	0.367
0.65	1.038	0.208	1.316	0.291	0.442
0.70	1.304	0.261	1.611	0.355	0.510
0.75	1.563	0.313	1.878	0.419	0.571
0.80	1.809	0.362	2.137	0.476	0.624
0.85	2.040	0.408	2.364	0.530	0.670
0.90	2.255	0.451	2.593	0.578	0.710
0.95	2.453	0.491	2.791	0.626	0.744
1.00	2.635	0.527	2.968	0.666	0.773

TABLE V. Total cross sections for $^{12}C(\overline{\nu}_\mu, \mu^+)$ scattering.

E (GeV)	$\sigma_{6p+6n}(E)$ (10^{-38} cm^2)				$\sigma_{\mathrm{FM+PB}}(E)$ (10^{-38} cm^2)			
	Resonance		+Background		Resonance		+Background	
	π^-	π^0	π^-	π^0	π^-	π^0	π^-	π^0
0.40	0.005	0.001	0.017	0.010	0.008	0.002	0.019	0.006
0.45	0.021	0.004	0.049	0.022	0.029	0.006	0.053	0.016
0.50	0.059	0.012	0.108	0.042	0.067	0.013	0.108	0.031
0.55	0.109	0.022	0.181	0.067	0.119	0.024	0.179	0.052
0.60	0.165	0.033	0.262	0.095	0.182	0.036	0.262	0.074
0.65	0.229	0.046	0.355	0.127	0.253	0.051	0.355	0.101
0.70	0.306	0.061	0.464	0.164	0.331	0.066	0.453	0.128
0.75	0.397	0.079	0.589	0.204	0.415	0.083	0.561	0.159
0.80	0.490	0.098	0.715	0.246	0.504	0.101	0.675	0.192
0.85	0.584	0.117	0.842	0.288	0.596	0.119	0.794	0.224
0.90	0.679	0.136	0.973	0.332	0.692	0.138	0.919	0.257
0.95	0.776	0.155	1.108	0.377	0.790	0.158	1.043	0.293
1.00	0.875	0.175	1.247	0.423	0.890	0.178	1.177	0.329

E (GeV)	$\sigma_{\Delta\ \text{in-medium}}(E)$ (10^{-38} cm^2)				Δ_{pionless}
	Resonance		+Background		
	π^-	π^0	π^-	π^0	
0.40	0.004	0.001	0.014	0.005	0.008
0.45	0.015	0.003	0.036	0.013	0.015
0.50	0.035	0.007	0.071	0.024	0.024
0.55	0.064	0.013	0.119	0.039	0.035
0.60	0.102	0.020	0.177	0.057	0.048
0.65	0.147	0.029	0.243	0.077	0.062
0.70	0.198	0.040	0.316	0.101	0.077
0.75	0.255	0.051	0.399	0.125	0.093
0.80	0.317	0.063	0.487	0.151	0.108
0.85	0.382	0.076	0.580	0.178	0.124
0.90	0.451	0.090	0.680	0.207	0.140
0.95	0.523	0.105	0.784	0.238	0.155
1.00	0.597	0.119	0.893	0.268	0.171

[1] J. Marteau, J. Delorme, and M. Ericson, Nucl. Instrum. Methods A **451**, 76 (2000); M. Martini, M. Ericson, G. Chanfray, and J. Marteau, Phys. Rev. C **80**, 065501 (2009); J. Nieves, I. Ruiz Simo, and M. J. Vicente Vacas, Phys. Lett. B **707**, 72 (2012).

[2] L. Alvarez-Ruso, Nucl. Phys. B, Proc. Suppl. **229-232**, 167 (2012).

[3] G. L. Fogli and G. Nardulli, Nucl. Phys. B **160**, 116 (1979).

[4] D. Rein, Z. Phys. C **35**, 43 (1987).

[5] E. Hernandez, J. Nieves, and M. Valverde, Phys. Rev. D **76**, 033005 (2007).

[6] D. Drechsel, S. S. Kamalov, and L. Tiator, Eur. Phys. J. A **34**, 69 (2007).

[7] C. Barbero, G. Lopez Castro, and A. Mariano, Phys. Lett. B **664**, 70 (2008).

[8] S. K. Singh, M. J. Vicente-Vacas, and E. Oset, Phys. Lett. B **416**, 23 (1998); **423**, 428(E) (1998).

[9] S. Ahmad, M. S. Athar, and S. K. Singh, Phys. Rev. D **74**, 073008 (2006); M. Sajjad Athar, S. Ahmad, and S. K. Singh, Nucl. Phys. A **782**, 179 (2007); S. K. Singh, M. Sajjad Athar, and S. Ahmed, AIP Conf. Proc. **967**, 182 (2007).

[10] M. Sajjad Athar, S. Chauhan, and S. K. Singh, J. Phys. G **37**, 015005 (2010); Eur. Phys. J. A **43**, 209 (2010).

[11] E. Oset and L. L. Salcedo, Nucl. Phys. A **468**, 631 (1987).

[12] S. J. Barish *et al.*, Phys. Rev. D **19**, 2521 (1979).

[13] G. M. Radecky *et al.*, Phys. Rev. D **26**, 3297 (1982); **26**, 3297(E) (1982).

[14] T. Kitagaki *et al.*, Phys. Rev. D **42**, 1331 (1990).

[15] A. Rodriguez *et al.*, Phys. Rev. D **78**, 032003 (2008).

[16] C. Mariani *et al.* (K2K Collaboration), Phys. Rev. D **83**, 054023 (2011).

[17] A. A. Aguilar-Arevalo *et al.* (MiniBooNE Collaboration), Phys. Rev. D **83**, 052007 (2011).

[18] A. A. Aguilar-Arevalo *et al.* (MiniBooNE Collaboration), Phys. Rev. D **83**, 052009 (2011).

[19] J. Nieves, I. R. Simo, and M. J. Vicente Vacas, Phys. Rev. C **83**, 045501 (2011).

[20] O. Lalakulich, E. A. Paschos, and G. Piranishvili, Phys. Rev. D **74**, 014009 (2006).

[21] J. Beringer *et al.* (Particle Data Group Collaboration), Phys. Rev. D **86**, 010001 (2012).

[22] D. Rein and L. M. Sehgal, Ann. Phys. **133**, 79 (1981).
[23] E. Hernandez, J. Nieves, S. K. Singh, M. Valverde, and M. J. Vicente Vacas, Phys. Rev. D **77**, 053009 (2008); M. Valverde, J. Nieves, E. Hernandez, S. K. Singh, and M. J. Vicente Vacas, Mod. Phys. Lett. A **23**, 2309 (2008).
[24] E. D. Bloom and F. J. Gilman, Phys. Rev. Lett. **25**, 1140 (1970).
[25] A. Gil, J. Nieves, and E. Oset, Nucl. Phys. A **627**, 543 (1997).
[26] M. Galassi, J. Davies, J. Theiler, B. Gough, G. Jungman, P. Alken, M. Booth, and F. Rossi, *GNU Scientific Library Reference Manual*, 3rd ed. (Network Theory Ltd., Godalming, UK, 2009).
[27] C. Praet, O. Lalakulich, N. Jachowicz, and J. Ryckebusch, Phys. Rev. C **79**, 044603 (2009).
[28] M. Antonello *et al.*, Acta Phys. Pol. B **40**, 2519 (2009).
[29] O. Lalakulich, K. Gallmeister, T. Leitner, and U. Mosel, AIP Conf. Proc. **1405**, 127 (2011).
[30] O. Lalakulich and U. Mosel, arXiv:1210.4717 [nucl-th].
[31] D. M. Manley and E. M. Saleski, Phys. Rev. D **45**, 4002 (1992).
[32] T. Leitner, Ph.D. thesis, Justus-Liebig-Universitaet Giessen, Fachbereich, 2007.
[33] M. El Amiri, J. Pestieau, and G. Lopez Castro, Nucl. Phys. A **543**, 673 (1992).
[34] V. Pascalutsa and R. Timmermans, Phys. Rev. C **60**, 042201 (1999).
[35] A. A. Aguilar-Arevalo *et al.* (MiniBooNE Collaboration), Phys. Rev. D **81**, 092005 (2010).
[36] C. Juszczak, J. A. Nowak, and J. T. Sobczyk, Nucl. Phys. Proc. Suppl. **159**, 211 (2006).
[37] O. Benhar, N. Farina, H. Nakamura, M. Sakuda, and R. Seki, Phys. Rev. D **72**, 053005 (2005).
[38] H. De Vries, C. W. De Jager, and C. De Vries, At. Data Nucl. Data Tables **36**, 495 (1987).
[39] C. Garcia-Recio, J. Nieves, and E. Oset, Nucl. Phys. A **547**, 473 (1992).
[40] S. Galster, H. Klein, J. Moritz, K. H. Schmidt, D. Wegener, and J. Bleckwenn, Nucl. Phys. B **32**, 221 (1971).
[41] L. Tiator, D. Drechsel, S. S. Kamalov, and M. Vanderhaeghen, Eur. Phys. J.: Spec. Top. **198**, 141 (2011).
[42] M. L. Goldberger and S. B. Treiman, Phys. Rev. **110**, 1178 (1958).
[43] S. L. Adler, Ann. Phys. (NY) **50**, 189 (1968).